Design and off-design optimisation of an organic Rankine cycle (ORC) system with an integrated radial turbine model

Sebastian Schuster[1], Christos N. Markides[2], and Alexander J. White[1]

[1]Department of Engineering, University of Cambridge, United Kingdom
[2]Clean Energy Processes (CEP) Laboratory, Department of Chemical Engineering, Imperial College London, United Kingdom

N.B.: This is the ACCEPTED MANUSCRIPT version of this article. The final, published version of the article can be found at: https://doi.org/10.1016/j.applthermaleng.2020.115192

Abstract

This paper investigates the design and thermodynamic optimisation of both sub- and trans-critical organic Rankine cycle (ORC) power systems featuring radial turbines via performance calculations using mean-line models. The emphasis is on rapid performance predictions for a given turbine geometry, as well as geometric optimisation for a given heat source. From three specified quantities, which are the turbine inlet temperature, inlet pressure and mass flow rate, the other flow properties (e.g., outlet pressure and temperature) are computed, together with derived quantities which are required for cycle- or system-level assessments, such as the isentropic efficiency of the turbine. Experimental investigations from the open literature suitable for validation purposes are summarised and analysed with respect to their strengths and weaknesses. Similar computational fluid dynamic (CFD) simulations are also used to complement the available experimental data. The main contributions of this paper are that it provides a comprehensive overview of radial turbine performance modelling, and that it proposes a detailed framework that can be used for the improved development of efficient thermodynamic power systems based on a unified mean-line model that is validated against experimental data and supported by CFD results. Specifically, predictions from the mean-line model show good accuracy over a wide range of operating conditions for different turbine designs and fluids with compressibility factors from 0.6 - 1.0. Finally, in order to demonstrate its efficacy, the integrated radial turbine and ORC system design framework is used in a case study of a nominally 400-kW power system with propane as the working fluid in low-grade waste-heat application, where the turbine inlet temperature is fixed at 150 °C and the condenser temperature is fixed at 15 °C. The novelty of this work arises from the optimisation of the turbine nozzle vane position at off-design conditions. This feature, along with multi-stage radial turbine designs are shown to allow high-performance operation over a wide range of off-design conditions. Specifically, good efficiencies are demonstrated over a wide range of heat-source fluid flow rates when employing an adjustable nozzle geometry, as is the ability of radial turbines to achieve efficiencies that are not constrained by the pressure ratio across them by replacing single-stage designs with multi-stage designs.

Nomenclature

The most important symbols used in this paper are listed below. All other symbols are defined in the text where they appear.

a	Speed of sound
A	Area
b	Channel width/blade height
c	Absolute velocity
Δh	Enthalpy change
$\dot{m}$	Mass flow rate
n	Rotational speed
N_N	Number of nozzle vanes
N_R	Number of rotor blades
p	Pressure
r	Radius
T	Temperature
u	Blade speed
w	Relative velocity
Z	Compressibility factor
α	Absolute flow angle
β	Relative flow angle
ϵ	Clearance
ϕ	Any variable
η	Efficiency
μ	Dynamic viscosity
ν	Tip-to-jet velocity ratio
Π	Pressure ratio
ρ	Density

Subscripts	
h	Hub
s	Isentropic change
l	Losses
m	In meridional direction
N	Nozzle
R	Rotor
0	Total conditions
t	Tip
ts	Total-to-static
θ	In tangential direction

1 Introduction

The production of electricity from fossil fuels, renewable sources, waste heat or even the storage of electricity itself requires careful attention to the underlying thermodynamic cycles if these energy sources are to be exploited efficiently and cost-effectively (Freeman et al. 2015, 2017). There are significant differences between these energy sources in terms of their magnitude, temporal variation and (in the case of thermal sources) their temperature. Consequently, different thermodynamic cycles are appropriate for their exploitation. For example, ORCs are deemed particularly suitable for low-to-medium temperature and small-to-medium scale waste heat re-

covery (Markides 2013, 2015, Colonna et al. 2015, Mahmoudi et al. 2018), whilst a range of solutions has been proposed for thermo-mechanical energy storage systems, including supercritical/transcritical CO_2 cyles (Mercangöz et al. 2012), Joule-Brayton based pumped thermal storage (Desrues et al. 2010, White et al. 2013, McTigue et al. 2015) and many others. In order to select and to design the best cycle and choose the most appropriate working fluid, the individual cycle components (heat exchangers (Karellas et al. 2012, Dong et al. 2017), compressors, expanders (Wu et al. 2015, Weiss et al. 2018, Hou et al. 2018), etc.) need to be modelled. Early-stage cycle design can be carried out with simple modelling methods involving relatively few parameters, such as an effectiveness for heat exchangers or a single isentropic (or polytropic) efficiency for compressors and expanders. Ultimately, however, more detailed information is required, and it is often necessary to know how a given component will perform over a range of operating conditions, away from its nominal design point. Thus, a detailed and reliable system analysis requires also in-depth understanding of the component models. Therefore, this paper contributes to the ORC system analysis by establishing and validating a component model for radial turbines as well as exploring the technical possibilities for part-load operation of the component and the system.

In the early stages of system design, the radial turbine is often incorported into the system calculation with an estimated peak efficiency, obtained by choosing two size parameters – for example the loading coefficient and the flow coefficient. For this purpose, Chen & Baines (1994) correlated the total-to-static efficiency of around 40 different radial turbines (most of them if not all operated with fluids behaving like ideal gases) with the loading and flow coefficients, thereby establishing that maximum efficiency can be reached for loading coefficients between 0.9 and 1.0 and flow coefficients between 0.2 and 0.3. The mean value of total-to-static efficiency in these ranges is around 87%. Similar maps have been compiled for organic fluids (Lazzaretto & Manente 2014, Lio et al. 2017). White & Sayma (2018) concluded that their data for different working fluids correlates well with the data of Chen & Baines (1994). White & Sayma (2019) presented a method that predicts the turbine design point efficiency only from the thermodynamic conditions and applied this model to cycle optimization, obtaining different optimum cycles with the new method compared to a fixed isentropic efficiency. The possiblity of generalising turbine performance data with reduced performance maps and similitude theory was studied extensively for ORC fluids by White & Sayma (2015*a*).

The aforementioned methods (size parameters, reduced performance maps, similitude theory) are a reliable and robust way to incorporate the turbine efficiency into thermodynamic cycle calculations and into the ORC system analysis if only the design point is considered, the number of design options is small, or the number of fluids is limited. Clearly a greater level of detail is required in order to model off-design behaviour and/or a larger number of fluids, that can even be designed during the cycle optimisation (Oyewunmi et al. 2017, White et al. 2018, van Kleef et al. 2019).

The aim of the present paper is to provide a validated calculation approach for radial turbines suitable for incorporation into cycle calculations with the intention to improve the ORC system analysis. (Note that the focus is on thermodynamic and aerodynamic performance – mechanical losses, electrical losses and costs are not considered here.) The paper starts with a review of the relevant experimental work and literature that gives comparison of experimental data with computations. The mean-line approach is then outlined, followed by validation against experimental data and supported by CFD calculations. Finally, the validated mean-line code is applied in the context of an ORC, considering both design and part-load behaviour to help exploring the technical possibilities offered by a radial turbine for on- and off-design operation of a whole ORC system.

The history of radial turbines spans several decades and for most purposes the technology is well understood. The associated literature is extensive, ranging from design approaches, mean-line and CFD analysis, to experimental verification. However, there are still phenomena, such as

condensation, that limit the operational range and that are not fully understood (see Schuster et al. (2018)), and studies on the impact of real gas effects are currently ongoing (e.g., Wheeler & Ong (2013, 2014), Durá Galiana et al. (2016), White et al. (2017)). Given the wide scope of this literature, the purpose of the present section is to give a broad but comprehensive overview of the work most relevant to mean-line modelling and to highlight the main findings.

The main experimental contributions come from Ricardo and Co., the NASA program, the Politecnico di Torino, Sundstrand and the Belfast program. Not all of these, however, provide sufficient information for the current purposes. Certain geometric information must be available to validate calculation methods. For mean-line calculations, the basic requirements for modelling isentropic changes include information on the nozzle inlet, tip and outlet diameter, the nozzle height and blade height, and the blade or flow angles. To model losses, the nozzle vane chord length, number of nozzle vanes, number of rotor blades, and clearances are all needed in addition. With this in mind, the following points apply to the above-mentioned list:

(i) The reports from Ricardo & Co. are not available in the open literature but a summary is given by Hiett & Johnston (1963). The geometry of the rotor is not fully described and the outlet blade angle is only given on an arbitrary diameter. Thus, the geometry can only be reproduced with certain assumptions.

(ii) NASA tested two radial turbines with tip diameters of 12 cm and 15 cm in the 1960s and early 1970s (Kofskey & Holeski 1966, Wasserbauer et al. 1966, Nusbaum & Wasserbauer 1967, Wasserbauer & Kofskey 1968, Futral & Holeski 1970, Futral & Wasserbauer 1970). The impact of rotational speed, Reynolds-number, tip clearance height and the use of splitter blades, mainly on the total-to-static efficiency, can be assessed from the NASA technical notes. An important finding from Nusbaum & Wasserbauer (1967) is that the peak total-to-static efficiency increases (by 2.1 percentage points) when the Reynolds number ($Re = \dot{m}/(\mu r_t)$) changes from 64 000 to 352 000. This efficiency change is rather small compared to the efficiency spectrum over a whole operational range.

Diameters and blade heights are fully described in the early NASA reports although some values must be derived. E.g. the nozzle height must be derived from the absolute and the relative rotor axial tip clearance. The design velocity triangles are given but nothing is said about the blade angles. Thus, to use the early NASA data for code validation assumptions must be made on either the blade angle or the flow angle (e.g., flow angles are equal to design flow angles).

(iii) In the later NASA publications (McLallin & Haas 1980, Simonyi et al. 1995) a full description of the radial turbine geometry is provided. Therefore, these cases can be used for mean-line model validation as well as for CFD code validation. The first publication is more promising since the whole operational range is investigated instead of a single point.

(iv) The Politecnico di Torino paper (Dadone & Pandolfi 1969) is missing information on the nozzle inlet. Thus, the nozzle losses cannot be calculated. Also, no information on the rotor clearance is given, so the results are not suitable for validation.

(v) In the Sunstrand paper (Jones 1994), measured values are given for the total-to-static and the total-to-total efficiency over a range of pressure ratios and rotational speeds while the mass flow rate is only given for one operation point. This is a drawback compared to the NASA investigations.

(vi) Plots of measured efficiency in the Belfast program (Spence & Artt 1997, Artt & Spence 1998, Spence et al. 1999, Doran et al. 2001, Spence et al. 2007) show qualitatively different behaviour from the above-mentioned measurement campaigns. Since no information is disclosed to fully reproduce the geometry, an in-depth analysis for this difference is not possible and so these results are not considered further.

(vii) Recently, the growing interest in ORC technology has pushed experimental investigations on radial turbines working with ORC fluids forward, and Kang (2012) found maximum turbine efficiencies above 80% for a turbine working with R245fa, while Shao et al. (2017) reported an efficiency value of 85% for a turbine working with R123a. These developments suggest that in the near future experiments on ORC turbines with fully disclosed geometries will be available for further validation.

In summary, the NASA, Ricardo & Co. and Jones data are most promising for code validation due to the availability and completeness of the data.

Besides the experimental investigations, mean-line and CFD program developments have a direct impact on this paper. For instance, Wasserbauer & Glassman (1975) described a mean-line program that requires the nozzle and rotor loss coefficients at the design point to be specified. Together with certain geometric values the off-design performance can be computed. These are in excellent agreement with the experimental results of Nusbaum & Kofskey (1969) and Wasserbauer et al. (1966).

Simonyi & Boyle (1991) compared quasi-3D calculation results with experiment. The computed total-total efficiency is four percentage points higher than the measured values. The slope of the efficiency curve plotted as a function of the pressure ratio also shows a considerable discrepancy, which they trace back to an uncertainty in the incidence loss model.

Baines (2005) compared the Ricardo & Co. results with a mean-line model and achieved excellent agreement. In a later publication (Qiu & Baines 2007) mean-line results are compared to experimental results from Ricardo & Co. and NASA and although the agreement is mostly excellent, the authors state that some tuning of the modelling parameters is required to achieve this. In particular, agreement with the C80 case was poor and required a very large increase in the rotor passage loss to match the measured efficiency (Qiu & Baines 2007). Persky & Sauret (2019) compare 1.5 million loss model configurations applied to a radial turbine working with either R134a or CO_2 and concluded that only a few are suitable to predict the turbine efficiency at off-design conditions.

The Jones data are widely used for CFD code validation since Sauret (2012) rediscovered this case and presented CFD results. Several authors (Sauret 2012, Keep et al. 2017, Al Jubori et al. 2017) predicted higher efficiencies of between two and four percentage points. Odabaee et al. (2014) however, calculated a considerably smaller efficiency by about 5-6 percentage points whilst Gad-el Hak et al. (2017) got a nearly perfect match (within 0.3 percentage points). These differences are at first surprising, given that they were obtained with the same CFD code, but most likely stem from uncertainties in specification of the geometry. Only Anderson & Bonhaus (2014) compared CFD results to the experiments for the Ricardo & Co. R70B turbine. Excellent agreement was obtained but, again, nothing is said about how the geometry was reproduced. Finally, Wheeler & Ong (2014) compared CFD results to the experimental results obtained by McLallin & Haas (1980) for the fully-described turbine and predicted a total-to-static efficiency just 0.5 percentage points lower.

Mean-line as well as CFD methods are applied to ORC turbines in the literature. Rahbar et al. (2015*a*) show the difference in efficiency for different turbines. The present paper continues this by also considering two-stage turbines to overcome efficiency penalties at high pressure ratios/loading coefficients and extends the investigations to off-design operation. Integrated design programs are often checked for plausibility in terms of computed geomerty and efficiency against experimental results and other design programs (Ventura et al. 2012, Rahbar et al. 2015*b*). Thereby, Rahbar et al. (2015*b*) obtained a ratio of hub radii $r_{model}/r_{exp} = 1.2$ and an efficiency difference of 3 percentage points. In the present paper, the turbine design process is separated from the performance calculation, this eases the validation process since the experimental investigated geometry can be modelled directly in the mean-line program. Further, the validation can simply be extended to off-design conditions.

In order to optimise a turbine, different levels of detail are considered in the open literature:

Mean-line models can only be used to optimise the main geometry dimensions, e.g., diameters and the desired flow angles at inlet and outlet. A further optimisation can be done by 3D CFD as shown by Sauret & Gu (2014). White & Sayma (2015*b*) presents a method to predict the fluid velocity distribution inside the rotor passage with a reduced order model. Zheng et al. (2017) combine a design tool with CFD as well as with a mean-line off-design tool and general trends of turbine power and efficiency with changing rotational speed, pressure ratio, and turbine inlet temperature are shown. In continuation to the aforementioned studies, this paper extends the existing knowledge by applying and optimising adjustable nozzle guide vanes to maximise cycle efficiency at off-design operation.

The above literature act to motivate the present work where point iii) and iv) are the main contributions:

(i) Comparison and validation of a unified mean-line model for radial turbines against a range of experimental and CFD results in terms of pressure ratio and total-static isentropic efficiency including off-design operation considered with mass flow rate and rotational speed variation.

(ii) Integration of a validated mean-line model into an ORC system model that enables explorations of the off-design operation and performance of sub-critical and transcritical systems.

(iii) Extension of the suitable design point pressure ratio through the employment of multi-stage radial turbines.

(iv) Operation range extension of ORC systems by utilizing adjustable guide vanes.

2 Performance modelling

2.1 Description of the main features of radial turbines

A radial inflow turbine consists of nozzle vanes and a rotor, as depicted in Fig. 1. The left-hand figure shows the so-called meridional plot (a cut between the blades) and that on the right shows the blade-to-blade view (at roughly mid blade height) and provides an indication of the flow turning. This is important since all turbomachinery operates by changing angular momentum and hence turning the flow in the circumferential direction. This is further highlighted by the velocity diagrams drawn at rotor inlet (2) and outlet (3). Note that u is the blade velocity, c and w are the flow absolute and relative velocities respectively, and that the numbering follows the usual convention for turbomachines.

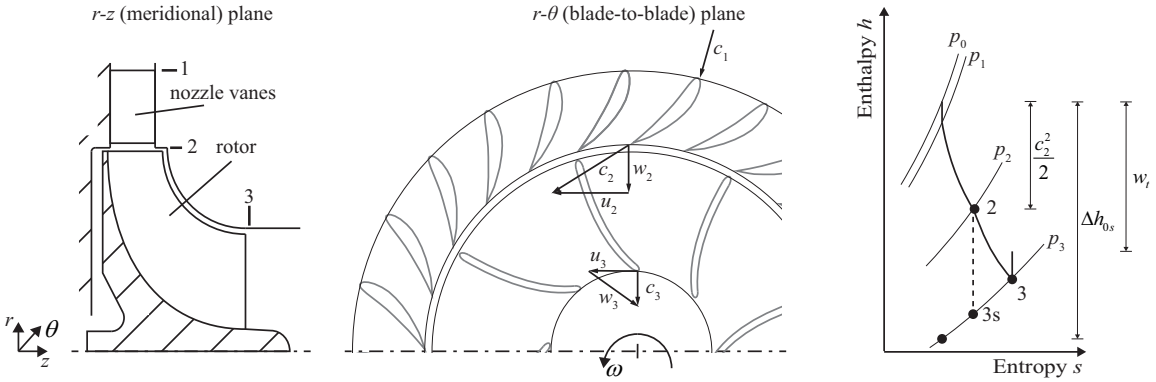


Figure 1: Sketch of a radial turbine with the typical calculation stations. The meridional plane is highlighting the main dimensions and the blade-to-blade plane gives insight into the flow turning. The $h - s$ diagram gives insight into the expansion process, especially highlighting nozzle outlet velocity c_2, total-static isentropic enthalpy change Δh_{0s}, and actual work output w_t.

2.2 Outline of the mean-line model

The backbone of the mean-line method is the Euler work equation which enables the specific work w_x delivered by a turbine (or absorbed by a compressor) to be calculated. It states that the 'rothalpy' $R = h_0 - uc_\theta$ is constant across a blade row, where $h_0 = h + 1/2c^2$ is the (absolute) stagnation enthalpy. The following procedure outlines how the mean-line method is applied across the rotor (similar steps apply to the stator):

(i) With the upstream conditions known and the mass flow $\dot{m}$ and rotor outlet flow angle β_3 specified, an initial estimate is made for the meridional exit velocity, c_{3m}.

(ii) The Euler work equation is applied to obtain an estimate of *actual* downstream static enthalpy:

$$h_3 = h_2 - \frac{1}{2}\left[c_{3m}^2\left(1+\tan^2\beta_3\right) + u_3^2 - c_{2m}^2\left(1+\tan^2\beta_2\right) - u_2^2\right]$$

(iii) The blade loss coefficient ζ (obtained from the loss model as a function of incidence angle, Reynolds number, etc., as detailed in Appendix A) is used to find the downstream *isentropic* enthalpy:

$$h_{3s} = h_3 - \frac{1}{2}\zeta c_3^2$$

(iv) The rotor exit pressure p_3 is unwrapped from an appropriate equation of state, using h_{3s} and $s_{3s} = s_2$. The density ρ_3 is then obtained from the *actual* enthalpy h_3 and p_3.

(v) Mass continuity is applied to obtain a new estimate for the meridional velocity, $c_{m3} = \dot{m}/(\rho_3 A_3)$, and steps (ii) to (v) are repeated until convergence – typically requiring 8-12 iterations.

This procedure is similar for all turbomachinery but there are some requirements specific to radial machines. The complexity and accuracy of the model are both affected by the selection and definition of suitable geometric parameters, flow turning angles and loss models. In particular, coupling between geometry and loss model definitions requires careful and consistent formulations. For the sake of reproducibility and completeness, full details are documented in Appendix A. Based on this model, a computational tool - hereafter named CAMRAD - has been established by the authors and is used for the following investigations.

2.3 Comparison with experimental data

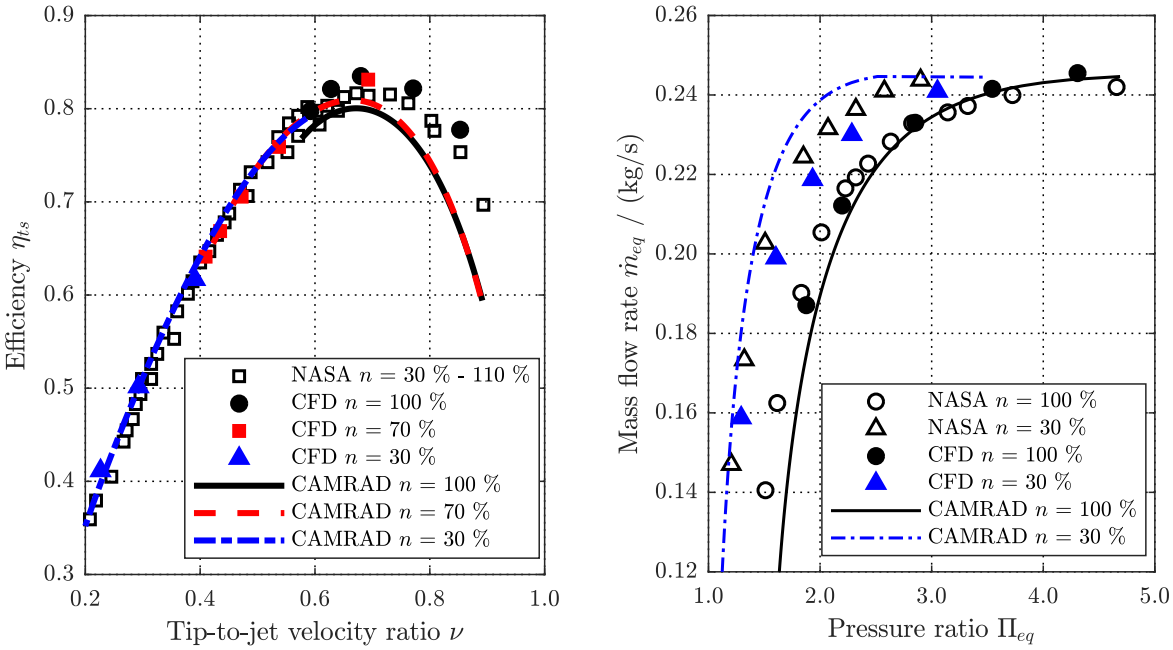
The mean-line model (CAMRAD) is validated by comparison with the most recent data from NASA and Ricardo. Performance is presented in terms of total-to-static efficiency η_{ts} versus tip-to-jet velocity ratio, $\nu = u_4/\sqrt{2\Delta h_{0t,6s}}$, and the pressure vs. mass flow characteristic. The latter is given in so-called 'equivalent' quantities, Π_{eq} and $\dot{m}_{eq}$, definitions of which are given in Appendix A. Input values for the mean-line calculation are given in Appendix B Table 4.

2.3.1 NASA 1980

McLallin & Haas (1980) give all the main details of their turbine including even blade surface co-ordinates and hence it is suitable for both mean-line and CFD code validation. The experimental (NASA), mean-line (CAMRAD) and CFD results are compared in Fig. 2. Mean-line results have been computed with flow angles taken from the measurements. The agreement in terms of total-to-static efficiency (Fig. 2a) is good up to the point of peak efficiency, beyond which the discrepancy is due to an overestimated incidence loss. This loss is notoriously difficult to predict; the correlation assumes complete dissipation of the tangential velocity component at rotor inlet, independent of whether the incidence is positive or negative. The results in Fig. 2a suggest that the dissipation is overpredicted, which in turn leads to an underestimation of the isentropic efficiency especially at higher tip-to-jet velocity ratios. (This aspect of loss modelling could possibly be improved with the help of CFD calculations.) The lower peak efficiency is most likely a result of overestimated passage and/or nozzle losses. These are captured by Reynolds-number correlations (details given in Appendix A) that work reasonable well for a set of turbines but are less able to capture the complex loss mechanisms accurately. These loss models are normally fitted to a specific turbine. For a different turbine the 'real' losses can be smaller, e.g., in an improved design resulting in an underestimated overall efficiency as can be observed here. The mass flow rate, however, is captured with reasonable accuracy over the whole operation range (Fig. 2b).

The CFD calculations are conducted with Ansys CFX and steady state calculations with second order spatial discretisation of one nozzle and one rotor passage with periodic boundary conditions and mixing interfaces are performed. The geometry of stator and impeller blades is directly reproduced from the surface co-ordinates provided in the publication of McLallin & Haas (1980) in conjunction with the co-ordinates of hub and shroud. The mesh is refined in four steps for one operation point and a max. difference in efficiency of 0.03 percentage points and a max. difference in mass flow rate of 0.3% for the last two refinements is found (an overview is given in Appendix C). The resulting efficiency obtained by CFD is higher than the measured values, the difference at the peak being about two percentage points. However, the variation with jet-to-tip velocity ratio is captured well, even in the high velocity regime. The CFD predictions of mass flow also match the experiments well at the design speed, but the deviations are more significant at part speed. This discrepancy is hard to explain, but it should be borne in mind that several assumptions (e.g., circumferential periodicity of the flow) have been applied. (the inlet nozzle vane height varies in the circumferential direction, but not enough information is given to create a 360° model of the geometry.)

In summary, good agreement for both CFD and mean-line results (and for both efficiency and mass flow data) lends confidence to these results. Furthermore, general trends for the mean-line method are supported by CFD, results from which might also be used to refine the loss models.



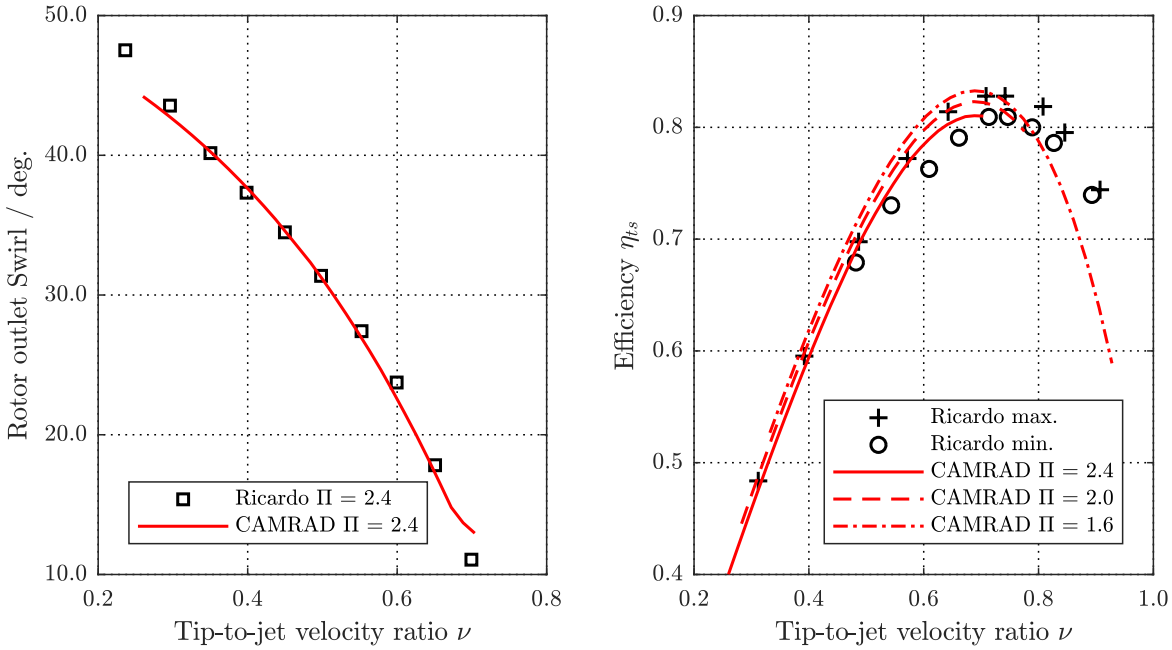
(a) Total-to-static efficiency

(b) Equivalent mass flow vs. pressure ratio

Figure 2: Experimental results from NASA (McLallin & Haas 1980) (open symbols) compared with CFD (filled symbols) and mean-line / CAMRAD (lines). The working fluid is air. Inlet total pressure and inlet total temperature are constant throughout the load point variation but exit pressure (and hence pressure ratio Π) and rotational speed n changes. Tip-to-jet velocity ratio ν is proportional to rotational speed and inverse to the pressure ratio (see Appendix A).

2.3.2 Ricardo turbine

The results for the Ricardo program are published by Hiett & Johnston (1963). The majority of information is given for Turbine B, including mass flow rate and efficiency measurements over a wide parameter range. The efficiency is determined from the torque measured by a dynamometer and hence includes disc friction and bearing losses. The missing information on the variation of rotor exit blade angle along the span is compensated by flow angle measurements. This are used to adjust the rotor outlet flow angle in the mean-line program to match the experimental data at one point ($\nu \approx 0.5$). As shown in Fig. 3, mean-line calculations of the rotor outlet swirl angle at approximately mid span and the total-to-static efficiency both agree well with measured values over a wide range of tip-to-jet ratios.



(a) Rotor exit swirl at $d = 0.5$ m, $\Pi = 2.4$

(b) Total-to-static efficiency for different Π

Figure 3: Comparison of experimental results for Ricardo Turbine B (symbols) with mean-line / CAMRAD calculations (lines) for lines of constant pressure ratio Π. The working fluid is air. Inlet total pressure, and inlet total temperature are kept constant, rotational speed and mass flow rate are changing. Tip-to-jet velocity ratio ν is proportional to rotational speed (see Appendix A).

2.3.3 NASA 1960s cases

Figure 4 shows comparison of measured total-to-static efficiency for the turbines of Kofskey & Holeski (1966) (KH) and Wasserbauer et al. (1966) (WKN) with calculations from the mean-line code. Agreement is very good for the WKN case but clearly not for the KH turbine. It is worth noting that these two turbines have similar geometry (they are scaled versions), and operate at very similar conditions in non-dimensional terms (see Table 1). The large differences in measured efficiencies are therefore unexpected and indeed the authors were unable to provide a definitive explanation. CFD was also unable to resolve this, but insufficient geometric details are available to create a reliable CFD model.

In conclusion to this section on validation, peak efficiency and trends of both efficiency and mass flow are for the most part well predicted by the mean-line method, to the extent that the method may be deemed suitable for design and off-design analysis in thermodynamic cycle codes.

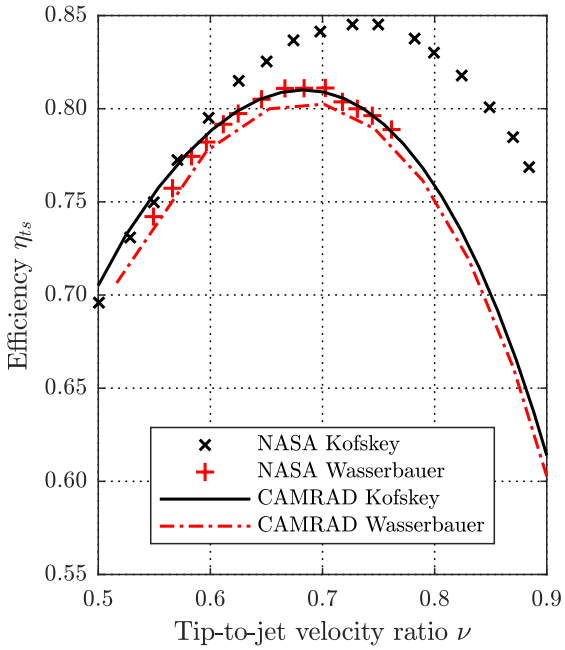


Figure 4: Comparison of the measured Kofskey (KH) and Wasserbauer (WKN) turbine efficiencies (NASA - symbols) with mean-line results (CAMRAD - lines). The working fluid is air for KH and argon for WKN. Rotational speed, inlet total pressure and inlet total temperature are constant for each turbine, but mass flow rate and pressure ratio are changing. Tip-to-jet velocity ratio ν is inverse to the pressure ratio.

Table 1: Design parameters for the NASA turbines.

	KH	WKN
Tip diameter d_4 / cm	15.3	11.7
Specific speed Ns	0.118	
Tip-to-jet velocity ratio ν	0.697	
Nozzle vanes	14 geometrically similar	
Rotor blades	11 geometrically similar	
Velocity triangles	identical	
Tip Reynolds number Re	63000 - 225000	82200
Axial clearance / mm	0.4826	0.2794
Radial clearance / mm	0.2540	0.3810

2.4 Comparison with CFD calculations

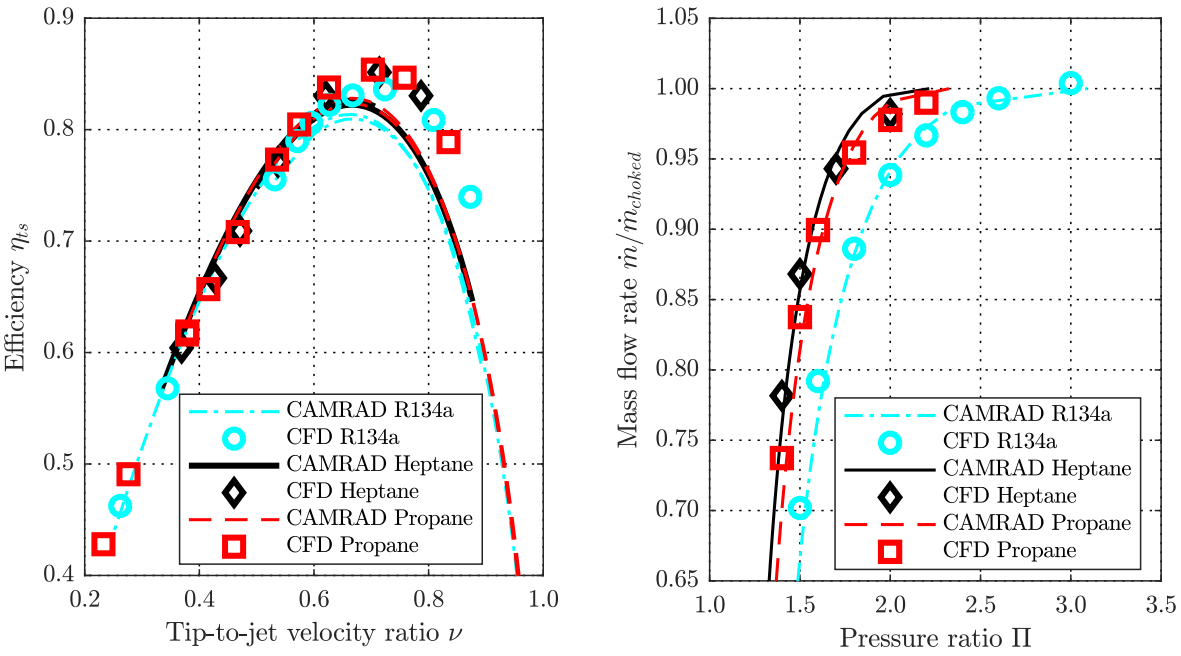
Mean-line results are compared to CFD simulations with the aim to increase confidence in the mean-line model for fluids that have a complex structure and/or do not obey the law of ideal gases. At the current state of research this is the best possibility to verify a mean-line model since the few experiments with 'real fluids' do not provide sufficient information about the turbine geometry to conduct mean-line calculations. The turbine geometry from McLallin & Haas (1980) with the CFD set-up already presented and summarised in Appendix C is used as a baseline given the fact that the CFD code has been validated for air already. Table 2 provides an overview on the investigated fluids, inlet boundary conditions, inlet compressibility factor, and isentropic outlet compressibility factor. Inlet pressure and temperature for R134a are equal to the air case, Heptane is selected as a long chain carbohydrate, and inlet conditions for propane are chosen from the ORC example provided in the next paragraph. The fluid properties are incorporated into the mean-line model directly with the REFPROP library (Lemmon et al. 2007) and into the

CFD code with look-up tables generated from the REFPROP library. Geometry input values for the mean-line calculations are given in Appendix B Table 4.

Table 2: Fluids, inlet boundary conditions, compressibility factor at inlet Z_0 and outlet Z_s

Fluid	p_{t0} / Pa	T_{t0} / K	Z_0	$Z_s(\Pi = 2)$
R134a	1.379×10^5	322.2	1.0	1.0
Heptane	26.0×10^5	593.15	0.72	0.85
Propane	65.6×10^5	423.0	0.59	0.70

The total-static efficiency for the three 'real fluids' shown in Fig. 5a follows the same trend already observed for the turbine operated with air. Again the incidence losses at tip-to-jet velocity ratios above the optimum value are over-predicted. The difference in peak efficiency is 2.1 percentage points for R134a, 2.9 percentage points for Heptane, and 3.1 percentage points for propane. This is similar to the difference obtained for air which is 3.5 percentage points. Since for the air turbine CFD over-predicts the peak-efficiency compared to the measurements and mean-line under-predicts it, the agreement between CFD and mean-line obtained for 'real fluids' is sufficient. Mass flow rate vs. pressure ratio shown in Fig. 5b is captured well. These results allow to conclude that the mean-line model provides sufficiently correct results even for molecules more complex than the components of air and for compressibility factors considerable different from one.



(a) Total-to-static efficiency obtained by changing outlet pressure and rotational speed

(b) mass flow vs. pressure ratio at fixed rotational speed for the particular fluid

Figure 5: CFD results (symbols) compared with mean-line / CAMRAD (lines) for different working fluids and compressibility factors Z between 0.6 and 1.0. Mass flow rate is normalized by the maximum value (choked nozzles) obtained with the mean-line (CAMRAD) model for the particular fluid.

3 Application to non-regenerative ORC system

The validated mean-line model is now applied to a non-regenerative ORC system to investigate the most suitable pressure ratio range and the impact of part-load operation on the cycle efficiency. Since the focus of this work is on the radial turbine, other components are modelled using very simple approaches. For example, the turbine inlet temperature is assumed fixed at 423 K (i.e., the dynamics of the main heat exchanger are not considered), but a 5% pressure loss is assumed in both the heat exchanger and condenser. The pump is assumed to have an isentropic efficiency of 80%. An ORC system with a nominal power output of 400 kW is considered, with propane as the working fluid and a condenser temperature of 288 K. This fixes the lower pressure at 7.3 bar. REFPROP (Lemmon et al. 2007) is used to incorporated the fluid properties into the mean-line model. From the large number of possible fluids, propane is chosen as the working fluid for this example since it has been used in other studies for low-temperature ORCs before (White et al. 2018, van Kleef et al. 2019, Nandaliarasyad et al. 2020).

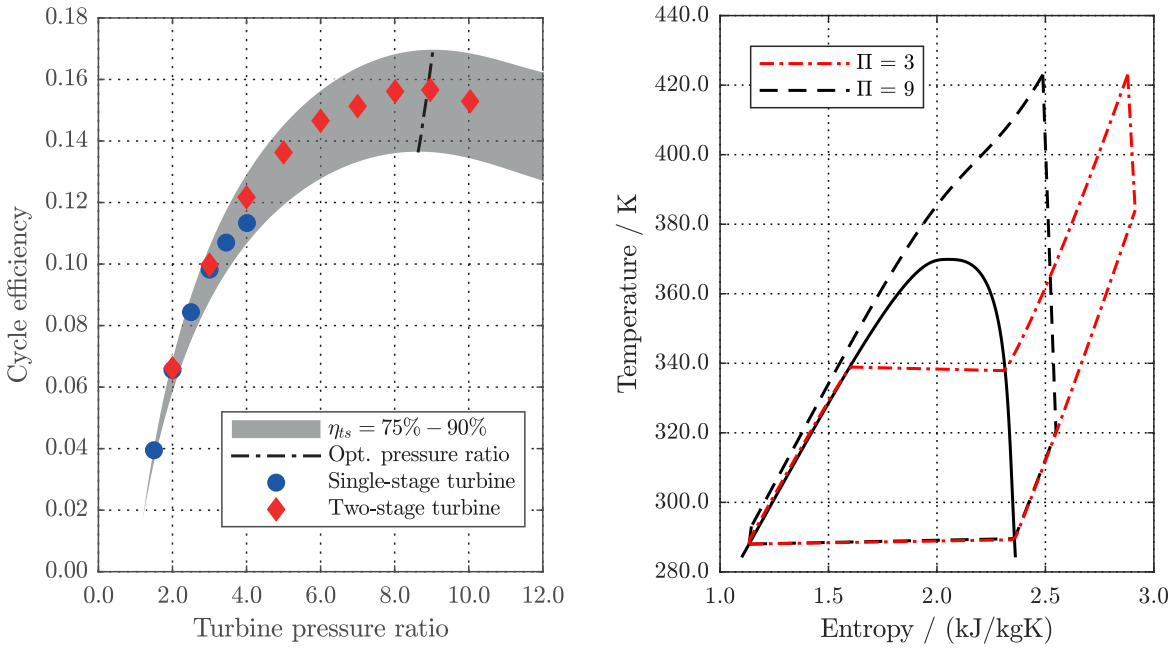
Based on the literature, peak isentropic efficiencies for radial turbines are in the range $\eta_t s$ = 75% to 90%. Figure 6a shows the ORC thermal efficiency as a function of pressure ratio for values of η_t in this range (grey shaded region), from which it is clear that the optimum pressure ratio for maximum cycle efficiency is around 9:1. (If, instead of efficiency, work output or cost were the objective function, the optimum cycle ratio would be lower.) Such high pressure ratios require either supersonic flow conditions or two-stage designs where the latter is applied for the high pressure ratios in the following paragraph.

3.1 Turbine optimisation for the design mass flow rate

The mean-line model allows a more realistic prediction of turbine performance than a simple, fixed isentropic efficiency, and is therefore useful in selection of the design point. In the present example the geometry is based on that investigated experimentally by McLallin & Haas (1980) and is optimised for different pressure ratios by varying the diameter, rotational speed, nozzle vane exit angle and rotor outlet angle. The MATLAB optimiser 'fmincon' (MATLAB 2017) has been used to find the parameter combination that gives the best isentropic total-to-static efficiency. For a single stage turbine this results in the cycle efficiencies shown as blue dots in Fig. 6a. The maximum pressure ratio cannot be higher than four since this requires acceleration in the nozzle vanes to supersonic conditions which cannot be achieved with a conventional design. (At high pressure ratios the turbine efficiency drops slightly due to high acceleration in the nozzle vanes and hence higher losses.)

To achieve the required pressure ratio, two turbine stages (HP, LP) are used. These have different optimum rotor diameters and rotational speeds. The combined isentropic efficiency of the two-stage turbine (red diamonds in Fig. 6a) for the cycle with the best efficiency is 84%. The resulting state point variations are illustrated in Fig. 6b and the main turbine geometric parameters for this design point calculation are given in Table 3.

The two stage design can be realised by two separate radial turbines each with inlet volute, nozzle guide vanes, impeller, and exit diffuser as well as a piping connection between the outlet diffuser of the first turbine and the volute inlet of the second. They can be coupled by a gear box to one generator. In this study, the additional losses in the piping between the two turbines are not included since it is estimated that they are small relative to the pressure drops inside the turbine stages. This is due to low fluid velocities and a short pipe length between the two stages. Further, by considering total-static efficiencies we already assume that the outlet kinetic energy is dissipated.



(a) Variation of overall cycle efficiency

(b) T-s diagrams at different pressure ratios

Figure 6: Impact of turbine pressure ratio on the achievable non-recuperative ORC system efficiency with a nominal power output of ≈ 400 kW and cycle as depicted in a $T - s$ diagram. Condenser temperature (288 K), upper cycle temperature (423 K), pump efficiency (80%), relative pressure losses (5%) in heat exchangers, mass flow rate (5 kg/s), and propane as working fluid are fixed. The mean-line model is used at each pressure ratio to optimise a turbine and the resulting isentropic turbine efficiency is used in the cycle calculation to obtain the depicted cycle efficiency.

Table 3: Main turbine geometry parameters resulting from the turbine optimisation. Single-stage turbine for Π=3 and two-stage turbine for Π=9 divided into high-pressure (HP) and low-pressure (LP) turbine.

Prop.	$\Pi = 3$	$\Pi = 9$, HP	$\Pi = 9$, LP
Tip diameter d / m	0.160	0.089	0.156
Rotational speed n / RPM	30500	46600	28500
Nozzle exit angle α / deg.	14.2	13.0	13.2
Rotor exit angle β / deg.	33.0	31.6	31.8

3.2 Load point variation

With the geometry fixed on the basis of the design point, the off-design operation can now be investigated. Load point variation is conducted here in order to determine the impact on cycle performance due to variations in turbine efficiency and pressure ratio. These have a similar impact on the cycle efficiency and both therefore need to be considered. Other component efficiencies and pressure drops are kept constant in order to isolate the effects of the turbine.

There are clearly several practical reasons why the cycle may need to operate away from its design point, including variations in the heat supply rate and in power demand. As a simple example here we consider a fixed turbine inlet temperature and vary the working fluid mass flow rate. This corresponds to variation in the heat source fluid flow rate (and the power output), but would also, ordinarily, result in changes to the turbine pressure ratio. This can be mitigated

by varying either the rotational speed and/or using adjustable nozzle vanes. Only the second possibility is considered here since changing the rotational speed (at least in the context of electricity generation) implies additional costs for the frequency converter.

3.2.1 Basic considerations

The change of pressure ratio with mass flow rate is most readily explained by considering the velocity triangles (Fig. 7) in conjunction with the Euler work equation, $\Delta h_0 = \Delta(uc_\theta)$. A common design approach is for the meridional velocity c_m to remain approximately constant through the machine, and to have zero swirl (c_θ) at exit from the rotor, as shown in Fig. 7(a). At reduced mass flow c_m is reduced but, for fixed geometry, the flow angles α and β are unchanged, resulting in a reduction in $c_{2\theta}$ and an increase in $c_{3\theta}$ (Fig. 7b). Since the blade speed is constant, there is a corresponding reduction in $\Delta(uc_\theta)$ and hence Δh_0 across both the rotor and the whole machine. This, in turn, results in a lower pressure ratio. However, by 'closing' the nozzle vanes (i.e., reducing α, as shown in Fig. 7c), $c_{2\theta}$ and $\Delta(uc_\theta)$ are partially restored, thereby recovering some of the reduction in pressure ratio. Similarly, the vanes can be 'opened' at high mass flow, though ultimately the flow is limited by choking at the rotor exit.

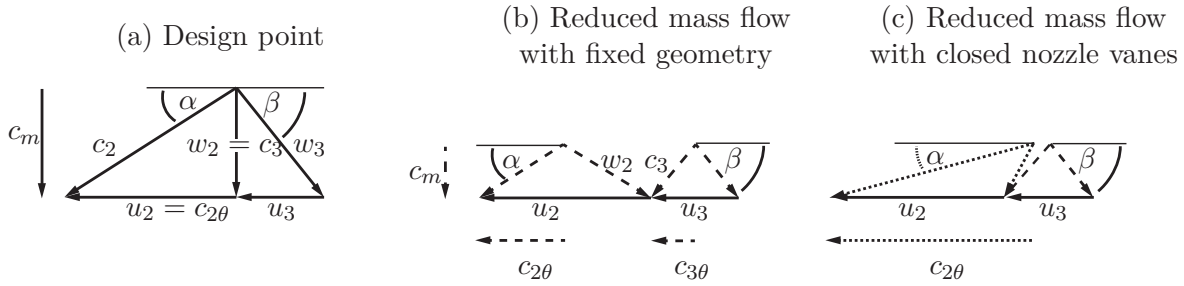
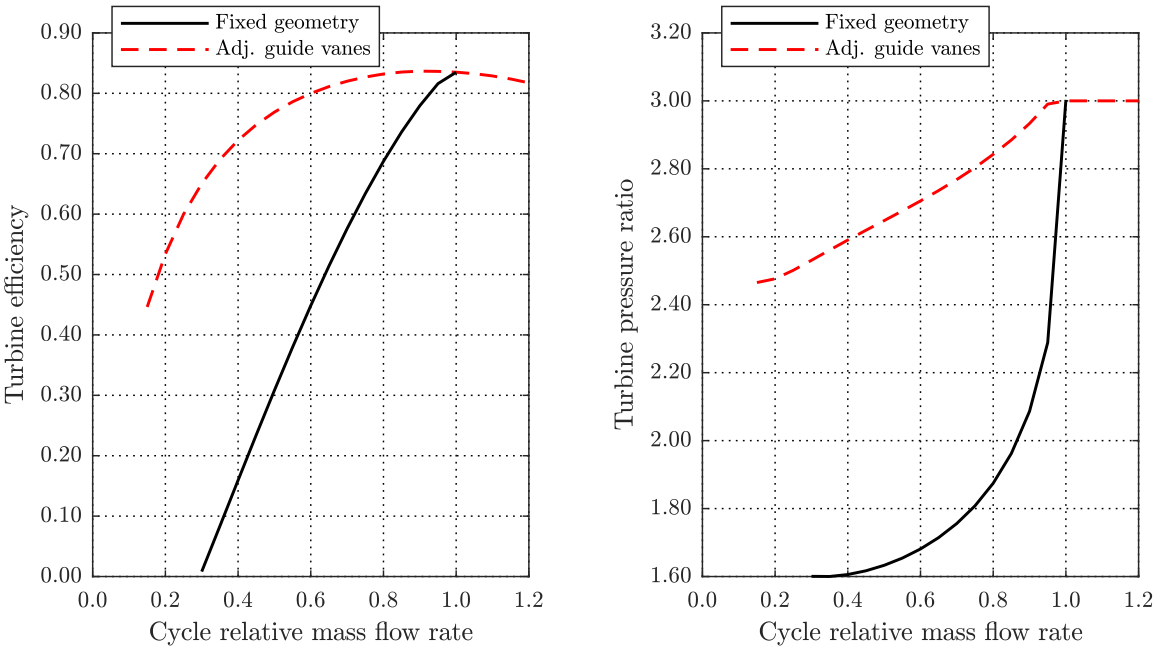


Figure 7: Velocity diagrams for different flow scenarios. With adjustable guide vanes (c) rotor incidence losses are kept low and $u_2 c_{2\theta}$ and hence turbine work and pressure ratio are kept high.

3.2.2 Performance map calculation with the mean-line model

As a final example of application of the mean-line model and its integration into cycle calculations, we consider the off-design operation of the ORC for both single- and two-stage turbine configurations and for both fixed and variable geometry. Departures from the design point are achieved by varying the mass flow of working fluid, as discussed above. The pressure ratio is allowed to drop below the design value, but not to exceed it as this would affect the pinch-point temperature and fundamentally change the cycle conditions. A case with fixed nozzle vane position is compared to a case with variable nozzle vane position. For the latter, the nozzle vane is rotated about a pivot point in order to change the blade angle and as a consequence the flow angle. The MATLAB optimiser 'fmincon' (MATLAB 2017) is applied to find the best vane position iteratively, where the objective function is maximum cycle efficiency for a specific cycle mass flow rate. In each inner loop, the mean line model CAMRAD is used to find the turbine pressure ratio and efficiency that in turn is used to compute the cycle efficiency.

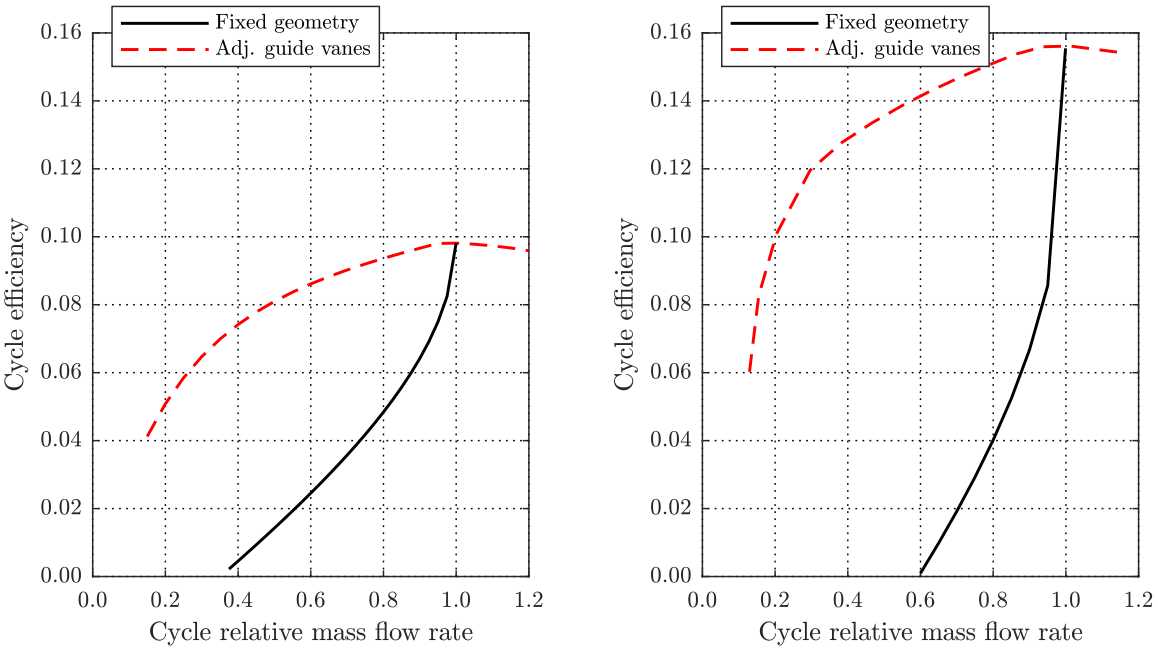


(a) Turbine efficiency (b) Pressure ratio

Figure 8: Effect of varying cycle mass flow rate on efficiency and pressure ratio of the single-stage turbine from the previous paragraphs. The mass flow rate of working fluid is changing and pressure ratio is allowed to drop below the design point value. For the fixed geometry efficiency and pressure ratio are only a function of mass flow rate but for adj. guide vanes mass flow rate and guide vane position are changing. Therefore, cycle efficiency is chosen as the objective function to find the best vane position.

Figure 8 shows the effect of varying the mass flow rate on the mean-line predictions of turbine (total-to-static) isentropic efficiency and pressure ratio for a single-stage machine, with and without nozzle-vane angle variation. For fixed geometry the losses become very large at low mass flow rate, such that the machine behaves effectively as a throttle and produces no useful work once $\dot{m}/\dot{m}_* \simeq 0.4$ (where $\dot{m}_*$ is the design mass flow). The extended range of operation achieved by the use of variable nozzle angles is quite notable, both in terms of turbine efficiency and pressure ratio. The vane angles have been chosen in this case so as to maximise the cycle efficiency, resulting in a variation that is roughly linear, with $\alpha \simeq 2 + 6\dot{m}/\dot{m}_*$, where α is in degrees. For the geometry considered here the maximum mass flow is limited not by choking but by practical constraints on the opening angle of the guide vanes, beyond which they would interfere with the rotor.

The one- and two-stage overall cycle efficiency variations are shown in Fig. 9. The operating range is clearly very restricted for the fixed-geometry cases since the reduction in both pressure ratio and turbine efficiency at reduced mass flow cause a precipitous fall in cycle efficiency. By contrast, the use of adjustable guide vanes enables a respectable cycle efficiency to be maintained at part load. For example, the cycle efficiency only fallen by 20% from its design value at relative mass flows of 45% and 35% for the single and two-stage cases respectively.



(a) Single stage turbine $\Pi_{Des} = 3$

(b) Two-stage turbine $\Pi_{Des} = 9$

Figure 9: Impact of load point variation realised by change of working fluid mass flow rate on cycle efficiency. The cycle pressure ratio is allowed to drop below the design value but not to exceed it. With adj. guide vanes both the turbine pressure ratio and efficiency can be maintained at higher values compared to the fixed geometry resulting in an overall higher cycle efficiency.

4 Conclusions

Motivated by the growing interest in ORC system design this paper presented a mean-line method for radial turbines with a specific view towards its application to thermodynamic cycle analysis. This has included a review of data and loss correlations available in the literature, which have subsequently been used to establish the mean-line model with a geometric description appropriate to radial machines. The model has been validated against a range of published experimental results for on- and off-design operation and CFD analysis. As part of its overall contribution, the method was applied to model the design and off-design operation of an ORC system. This study has revealed that multiple turbine stages are beneficial to extend the feasible cycle pressure ratio. A major contribution is the exploration of the part-load operation range of ORC systems equipped with radial inflow turbines as well as a method to extend this range. While the focus of this paper is on thermodynamic and aerodynamic performance aspects, the practical and economical feasibility of the presented technical solutions are also of great importance and need to be considered in future work. The methods and analysis provided in this paper can be used by the scientific community to assess the off-design operation of ORC systems with radial turbines for different applications and working fluids. This hopefully helps to explore a range of heat sources more efficiently.

Finally, the following conclusions can be drawn:

(i) With the exception of one geometry, good agreement between the mean-line model and available experimental data can be obtained in terms of turbine efficiency and pressure ratio vs. mass flow characteristics. In particular, the predicted part-load performance agrees acceptably well with the measured data, thereby confirming the suitability of the loss correlations.

(ii) Published experimental investigations of radial machines are limited to fluids that behave like ideal gases. There is a lack of data relating to the 'real fluids' commonly used in ORC applications.

(iii) The mean-line model allows prediction of the turbine efficiency that can be achieved and the required number of stages at the cycle design phase. Typically, optimisation in terms of diameter, rotational speed and flow angles gives a peak total-to-static isentropic efficiency of around 84%. For the investigated non-regenerative ORC system a two-stage turbine design is beneficial in terms of efficiency for pressure ratios greater than three.

(iv) For off-design operation, variation of the nozzle vane angles enables the mass flow to be varied over a wide range whilst retaining a reasonable cycle efficiency (e.g., for the two-stage case considered the cycle efficiency remains within 80% of its design value for flow rates between 35 and 120% of design). This enables the cycle to match commensurate variations in the flow rate of the heat source fluid.

5 Acknowledgements

This work was supported by the UK Engineering and Physical Sciences Research Council (EPSRC) [grant number EP/P004709/1]. Data supporting this publication can be obtained on request from cep-lab@imperial.ac.uk.

References

Al Jubori, A. M., Al-Dadah, R. & Mahmoud, S. (2017), 'New performance maps for selecting suitable small-scale turbine configuration for low-power organic Rankine cycle applications', *Journal of Cleaner Production* **161**, 931–946.

Anderson, M. R. & Bonhaus, D. L. (2014), Validation results for a diverse set of turbomachinery cases using a density-based OpenFOAM solver, *in* 'Proceedings of the ASME Turbo Expo', Vol. 2B.

Artt, D. W. & Spence, S. W. (1998), 'A loss analysis based on experimental data for a 99.0 mm radial inflow nozzled turbine with different stator throat areas', *Proceedings of the Institution of Mechanical Engineers, Part A: Journal of Power and Energy* **212**(1), 27–42.

Baines, N. (2005), 'Radial turbines: An integrated design approach', *ETC 2005 - 6th Conference on Turbomachinery: Fluid Dynamics and Thermodynamics* .

Chen, H. & Baines, N. C. (1994), 'The aerodynamic loading of radial and mixed-flow turbines', *International Journal of Mechanical Sciences* **36**(1), 63–79.

Colebrook, C. F. (1939), 'Turbulent flow in pipes, with particular reference to the transition region between the smooth and rough pipe laws', *Journal of the Institution of Civil Engineers* **11**(4), 133–156.

Colonna, P., Casati, E., Trapp, C., Mathijssen, T., Larjola, J., Turunen-Saaresti, T. & Uusitalo, A. (2015), 'Organic Rankine cycle power systems: From the concept to current technology, applications, and an outlook to the future', *Journal of Engineering for Gas Turbines and Power* **137**(10), 100801.

Dadone, A. & Pandolfi, M. (1969), 'A method for evaluating the off-design performance of a radial inflow turbine and comparison with experiments', *International Journal of Mechanical Sciences* **11**(3), 241–252.

Desrues, T., Ruer, J., Marty, P. & Fourmigue, J. (2010), 'A thermal energy storage process for large scale electric applications', *Applied Thermal Engineering* **30**(5), 425 – 432.

Dong, J., Zhang, X. & Wang, J. (2017), 'Experimental investigation on heat transfer characteristics of plat heat exchanger applied in organic rankine cycle (orc)', *Applied Thermal Engineering* **112**, 1137 – 1152.
URL: *http://www.sciencedirect.com/science/article/pii/S135943111632885X*

Doran, W. J., Spence, S. W. & Artt, D. W. (2001), 'Experimental performance evaluation of a 99.0 mm radial inflow nozzled turbine with varying shroud profiles', *Proceedings of the Institution of Mechanical Engineers, Part A: Journal of Power and Energy* **215**(2), 267–280.

Durá Galiana, F. J., Wheeler, A. P. & Ong, J. (2016), 'A study of trailing-edge losses in organic Rankine cycle turbines', *Journal of Turbomachinery* **138**(12), 121003.

Freeman, J., Hellgardt, K. & Markides, C. N. (2015), 'An assessment of solar-powered organic Rankine cycle systems for combined heating and power in UK domestic applications', *Applied Energy* **138**, 605–620.

Freeman, J., Hellgardt, K. & Markides, C. N. (2017), 'Working fluid selection and electrical performance optimisation of a domestic solar-ORC combined heat and power system for year-round operation in the UK', *Applied Energy* **186**, 291–303.

Futral, S. M. & Holeski, D. E. (1968), Experimental performance evaluation of a 6.02-inch (15.29-cm) radial-inflow turbine with an exit diffuser, number NASA TM X-1480 *in* 'NASA Technical Memorandum'.

Futral, S. M. & Holeski, D. E. (1970), Experimental results of varying the blade- shroud clearance in a 6.02-inch radial-inflow turbine, number TN D-5513 *in* 'NASA Technical Note'.
URL: *https://ntrs.nasa.gov/search.jsp?R=19700008458*

Futral, S. M. & Wasserbauer, C. A. (1970), Experimental performance evaluation of a 4.59-inch radial-inflow turbine with and without splitter blades, number TN D-7015 *in* 'NASA Technical Note'.
URL: *https://ntrs.nasa.gov/search.jsp?R=19710002790*

Gad-el Hak, I., Hussin, A., Hamed, A. & Mahmoud, N. (2017), '3D numerical modeling of zeotropic mixtures and pure working fluids in an ORC turbo-expander', *International Journal of Turbomachinery, Propulsion and Power* **2**(1), 2.

Glassman, A. J. (1976), Computer program for design analysis of radial-inflow turbines, number TN D-8164 *in* 'NASA Technical Note'.
URL: *https://ntrs.nasa.gov/archive/nasa/casi.ntrs.nasa.gov/19760010058.pdf*

Hiett, G. F. & Johnston, I. H. (1963), 'Experiments concerning the aerodynamic performance of inward flow radial turbines', *Proceedings of the Institution of Mechanical Engineers* (9), 28–42.

Hou, X., Zhang, H., Xu, Y., Tian, Y., Zhao, T., Li, J. & Yu, F. (2018), 'Performance investigation of a free piston expander-linear generator for small scale organic Rankine cycle', *Applied Thermal Engineering* **144**, 209 – 218.
URL: *http://www.sciencedirect.com/science/article/pii/S135943111831370X*

Jones, A. C. (1994), 'Design and test of a small, high pressure ratio radial turbine', *American Society of Mechanical Engineers* pp. 1–12.

Kang, S. H. (2012), 'Design and experimental study of ORC (organic Rankine cycle) and radial turbine using R245fa working fluid', *Energy* **41**(1), 514 – 524. 23rd International Conference on Efficiency, Cost, Optimization, Simulation and Environmental Impact of Energy Systems, ECOS 2010.

Karellas, S., Schuster, A. & Leontaritis, A.-D. (2012), 'Influence of supercritical orc parameters on plate heat exchanger design', *Applied Thermal Engineering* **33-34**, 70 – 76.
URL: *http://www.sciencedirect.com/science/article/pii/S1359431111004935*

Keep, J. A., Vitale, S., Pini, M. & Burigana, M. (2017), 'Preliminary verification of the open-source CFD solver SU2 for radial-inflow turbine applications', *Energy Procedia* **129**, 1071–1077.

Kofskey, M. G. & Holeski, D. E. (1966), Cold performance evaluation of a 6.02-inch radial inflow turbine designed for a 10-kilowatt shaft output Brayton cycle space power generation system, number TN D-2987 *in* 'NASA Technical Note'.
URL: *https://ntrs.nasa.gov/search.jsp?R=19660006767*

Lazzaretto, A. & Manente, G. (2014), 'A new criterion to optimize ORC design performance using efficiency correlations for axial and radial turbines', *International Journal of Thermodynamics* **17**, 192 – 200.

Lemmon, E. W., Huber, M. L. & McLinden, M. O. (2007), 'NIST Standard Reference Database 23: Reference Fluid Thermodynamic and Transport Properties-REFPROP, Version 8.0, National Institute of Standards and Technology'.
URL: *https://www.nist.gov/srd/refprop*

Lio, L. D., Manente, G. & Lazzaretto, A. (2017), 'A mean-line model to predict the design efficiency of radial inflow turbines in organic Rankine cycle (ORC) systems', *Applied Energy* **205**, 187 – 209.

Mahmoudi, A., Fazli, M. & Morad, M. (2018), 'A recent review of waste heat recovery by organic Rankine cycle', *Applied Thermal Engineering* **143**, 660 – 675.

Markides, C. N. (2013), 'The role of pumped and waste heat technologies in a high-efficiency sustainable energy future for the UK', *Applied Thermal Engineering* **53**(2), 197–209.

Markides, C. N. (2015), 'Low-concentration solar-power systems based on organic Rankine cycles for distributed-scale applications: Overview and further developments', *Frontiers in Energy Research* **3**.

MATLAB (2017), *version 9.3.0 (R2017b)*, The MathWorks Inc., Natick, Massachusetts.

McKoen, B. J., Swanson, C. J., Zagarola, M. V., Donnelly, R. J. & Smits, A. J. (1999), 'Friction factors for smooth pipe flow', *Journal of Fluid Mechanics* **511**, 41–44.

McLallin, K. L. & Haas, J. E. (1980), Experimental performance and analysis of 15.04-centimeter-tip-diameter, radial-inflow turbine with work factor of 1.126 and thick blading, number 1730 *in* 'Technical Paper'.

McTigue, J. D., White, A. J. & Markides, C. N. (2015), 'Parametric studies and optimisation of pumped thermal electricity storage', *Applied Energy* **137**, 800 – 811.

Mercangöz, M., Hemrle, J., Kaufmann, L., Z'Graggen, A. & Ohler, C. (2012), 'Electrothermal energy storage with transcritical CO_2 cycles', *Energy* **45**(1), 407 – 415. The 24th International Conference on Efficiency, Cost, Optimization, Simulation and Environmental Impact of Energy, ECOS 2011.

Moustapha, H., Zelesky, M. F. & Baines, N. C. (2003), *Axial and Radial Turbines*, Concepts ETI, White River Junction, Vt.

Nandaliarasyad, N., Maulana, D. T. & Darmanto, P. S. (2020), 'Study of development scenarios for bottoming unit binary cycle to utilize exhaust steam from back pressure turbine geothermal power plant', *IOP Conference Series: Earth and Environmental Science* **417**, 012017.
URL: *https://doi.org/10.1088/1755-1315/417/1/012017*

Nusbaum, W. J. & Kofskey, M. G. (1969), Cold performance evaluation of 4.97-inch radial-inflow turbine designed for single-shaft Brayton cycle space power system, number TN D-5090 *in* 'NASA Technical Note'.

Nusbaum, W. J. & Wasserbauer, C. A. (1967), Experimental performance evaluation of a 4.59-inch radial-inflow turbine over a range of Reynolds number, number TN D-3835 *in* 'NASA Technical Note'.
URL: *https://ntrs.nasa.gov/search.jsp?R=19670008297*

Odabaee, M., Sauret, E. & Hooman, K. (2014), 'Computational fluid dynamics simulation and turbomachinery code validation of a high pressure ratio radial-inflow turbine', *10th International Conference on Heat Transfer, Fluid Mechanics and Thermodynamics (HEFAT2014), HEFAT, Orlando, Florida, USA.* .

Oyewunmi, O. A., Kirmse, C. J., Pantaleo, A. M. & Markides, C. N. (2017), 'Performance of working-fluid mixtures in ORC-CHP systems for different heat-demand segments and heat-recovery temperature levels', *Energy Conversion and Management* **148**, 1508 – 1524.

Persky, R. & Sauret, E. (2019), 'Loss models for on and off-design performance of radial inflow turbomachinery', *Applied Thermal Engineering* **150**, 1066 – 1077.

Qiu, X. & Baines, N. (2007), Performance prediction for high pressure-ratio radial inflow turbines, *in* 'Proceedings of the ASME Turbo Expo', Vol. 6 PART B, pp. 945–956.

Rahbar, K., Mahmoud, S., Al-Dadah, R. K. & Moazami, N. (2015*a*), 'Modelling and optimization of organic Rankine cycle based on a small-scale radial inflow turbine', *Energy Conversion and Management* **91**, 186 – 198.

Rahbar, K., Mahmoud, S., Al-Dadah, R. K. & Moazami, N. (2015*b*), 'Parametric analysis and optimization of a small-scale radial turbine for organic Rankine cycle', *Energy* **83**, 696 – 711.

Rodgers, C. (1987), 'Mainline performance prediction for radial inflow turbines'.

Sauret, E. (2012), Open design of high pressure ratio radial-inflow turbine for academic validation, *in* 'ASME International Mechanical Engineering Congress and Exposition, Proceedings (IMECE)', Vol. 7, pp. 3183–3197.

Sauret, E. & Gu, Y. (2014), 'Three-dimensional off-design numerical analysis of an organic Rankine cycle radial-inflow turbine', *Applied Energy* **135**, 202 – 211.

Schlichting, H. & Gersten, K. (2003), *Boundary-layer theory*, Physics and astronomy online library, 8., rev. and enl. ed., corr. print edn, Springer, Berlin.

Schuster, S., Brillert, D. & Benra, F.-K. (2018), 'Condensation in radial turbines – part II: Application of the mathematical model to a radial turbine series', *Journal of Turbomachinery* **140**(10).

Shao, L., Zhu, J., Meng, X., Wei, X. & Ma, X. (2017), 'Experimental study of an organic Rankine cycle system with radial inflow turbine and R123', *Applied Thermal Engineering* **124**, 940 – 947.
URL: *http://www.sciencedirect.com/science/article/pii/S1359431117339200*

Simonyi, P. & Boyle, R. (1991), Comparison of a quasi-3D analysis and experimental performance for three compact radial turbines.
URL: *https://ntrs.nasa.gov/search.jsp?R=19910020828*

Simonyi, S. R., Roelke, R. J., Stabe, R. G., Nowlin, B. C. & DiCicco, D. (1995), Aerodynamic evaluation of two compact radial-inflow turbine rotors, number TP-3514 *in* 'NASA Technical Paper'.
URL: *https://ntrs.nasa.gov/search.jsp?R=19960003236*

Spence, S. W. & Artt, D. W. (1997), 'Experimental performance evaluation of a 99.0 mm radial inflow nozzled turbine with different stator throat areas', *Proceedings of the Institution of Mechanical Engineers, Part A: Journal of Power and Energy* **211**(6), 477–488.

Spence, S. W., Doran, W. J. & Artt, D. W. (1999), 'Experimental performance evaluation of a 99.0 mm radial inflow nozzled turbine at larger stator-rotor throat area ratios', *Proceedings of the Institution of Mechanical Engineers, Part A: Journal of Power and Energy* **213**(3), 205–218.

Spence, S. W., Rosborough, R. S., Artt, D. & McCullough, G. (2007), 'A direct performance comparison of vaned and vaneless stators for radial turbines', *Journal of Turbomachinery* **129**(1), 53–61.

Suhrmann, J. F., Peitsch, D., Gugau, M., Heuer, T. & Tomm, U. (2010), Validation and development of loss models for small size radial turbines, *in* 'Proceedings of the ASME Turbo Expo', pp. 1937–1949.

van Kleef, L. M., Oyewunmi, O. A. & Markides, C. N. (2019), 'Multi-objective thermo-economic optimization of organic Rankine cycle (ORC) power systems in waste-heat recovery applications using computer-aided molecular design techniques', *Applied Energy* **251**, 112513.

Ventura, C. A., Jacobs, P. A., Rowlands, A. S., Petrie-Repar, P. & Sauret, E. (2012), 'Preliminary design and performance estimation of radial inflow turbines: An automated approach', *Journal of Fluids Engineering* **134**(3).

Wasserbauer, C. A. & Glassman, A. J. (1975), Fortran program for predicting off-design performance of radial-inflow turbines, number TN D-8063 *in* 'NASA Technical Note'.
URL: *https://ntrs.nasa.gov/archive/nasa/casi.ntrs.nasa.gov/19750024045.pdf*

Wasserbauer, C. A. & Kofskey, M. G. (1968), Aerodynamic performance of a 4.59-inch modified radial-inflow turbine for a single-shaft Brayton cycle space power system, number TM X-1615 *in* 'NASA Technical Memorandum'.
URL: *https://ntrs.nasa.gov/search.jsp?R=19680019398*

Wasserbauer, C. A., Kofskey, M. G. & Nusbaum, W. J. (1966), Cold performance evaluation of a 4.59-inch radial-inflow turbine designed for a Brayton-cycle space power system, number TN D-3260 *in* 'NASA Technical Note'.
URL: *https://ntrs.nasa.gov/search.jsp?R=19660006353*

Weiss, A. P., Popp, T., Mueller, J., Hauer, J., Brueggemann, D. & Preissinger, M. (2018), 'Experimental characterization and comparison of an axial and a cantilever micro-turbine for small-scale organic Rankine cycle', *Applied Thermal Engineering* **140**, 235 – 244.
URL: *http://www.sciencedirect.com/science/article/pii/S1359431118302035*

Wheeler, A. P. S. & Ong, J. (2013), 'The role of dense gas dynamics on organic Rankine cycle turbine performance', *Journal of Engineering for Gas Turbines and Power* **135**(10), 102603.

Wheeler, A. P. S. & Ong, J. (2014), A study of the three-dimensional unsteady real-gas flows within a transonic ORC turbine, *in* 'Proceedings of the ASME Turbo Expo', p. V03BT26A003.

White, A., Parks, G. & Markides, C. N. (2013), 'Thermodynamic analysis of pumped thermal electricity storage', *Applied Thermal Engineering* **53**(2), 291–298.

White, M. & Sayma, A. I. (2015*a*), 'The application of similitude theory for the performance prediction of radial turbines within small-scale low-temperature organic Rankine cycles', *Journal of Engineering for Gas Turbines and Power* **137**(12).

White, M. & Sayma, A. I. (2015*b*), The one-dimensional meanline design of radial turbines for small scale low temperature organic Rankine cycles, *in* 'Proceedings of the ASME Turbo Expo', Vol. 2C.

White, M., Sayma, A. I. & Markides, C. N. (2017), 'Supersonic flow of non-ideal fluids in nozzles: An application of similitude theory and lessons for ORC turbine design and flexible use considering system performance', *Journal of Physics: Conference Series* **821**, 012002.

White, M. T., Oyewunmi, O. A., Chatzopoulou, M. A., Pantaleo, A. M., Haslam, A. J. & Markides, C. N. (2018), 'Computer-aided working-fluid design, thermodynamic optimisation and thermoeconomic assessment of ORC systems for waste-heat recovery', *Energy* **161**, 1181 – 1198.

White, M. T. & Sayma, A. I. (2018), 'A generalised assessment of working fluids and radial turbines for non-recuperated subcritical organic Rankine cycles', *Energies* **11**(4).

White, M. T. & Sayma, A. I. (2019), 'Simultaneous cycle optimization and fluid selection for ORC systems accounting for the effect of the operating conditions on turbine efficiency', *Frontiers in Energy Research* **7**, 50.

Wu, Z., Pan, D., Gao, N., Zhu, T. & Xie, F. (2015), 'Experimental testing and numerical simulation of scroll expander in a small scale organic Rankine cycle system', *Applied Thermal Engineering* **87**, 529 – 537.
URL: *http://www.sciencedirect.com/science/article/pii/S1359431115004858*

Zheng, Y., Hu, D., Cao, Y. & Dai, Y. (2017), 'Preliminary design and off-design performance analysis of an organic Rankine cycle radial-inflow turbine based on mathematic method and CFD method', *Applied Thermal Engineering* **112**, 25 – 37.

Appendix A Full details of mean-line model

For cycle calculations the performance estimation of radial turbines has to be quick, reliable and flexible regarding main geometry parameter variations. These requirements can be fulfilled by a mean-line calculation approach. In this the complexity of the three dimensional flow through a radial turbine is greatly reduced by assuming a steady state flow process, averaging the flow in circumferential direction, and averaging the flow in the geometric span wise direction. Further, calculations are only performed at a certain number of stations, e.g., stator inlet, stator outlet respectively rotor inlet, and rotor outlet.

In the mean-line model used in this paper pressure ratio and efficiency are evaluated for given inlet total conditions and mass flow rate. The change of flow variables is calculated at four stations according to Fig. 10 with the nozzles located between 1 and 3 and the rotor between 4 and 6. Not considered are the stations 2 and 5 which can be located within the bladed space to account for blockage. The numbering convention and symbols follow the commonly used system in the literature.

The velocity triangles at the impeller inlet and outlet are shown in the right part of the figure and the definition of stations, velocities and angles is used throughout this section. Further, the hydraulic diameter of the passage D_h is based on Moustapha et al. (2003, p. 226, Eq. 8.31) but formulated with the rotor exit radii $r_{6,t/h}$ instead of the throat radii $r_{5,t/h}$ as:

$$D_h = \frac{2\pi r_4 b_4}{2\pi r_4 + N_R b_4} + \frac{\pi(r_{6,t}^2 - r_{6,h}^2)}{\pi(r_{6,t} - r_{6,h}) + N_R(r_{6,t} - r_{6,h})}, \tag{1}$$

with N_R being the number of rotor blades. The passage length l_m (Glassman 1976, p. 53, Eq. C2) is:

$$l_m = \frac{\pi}{2}\sqrt{\frac{1}{2}\left[\left(r_4 - r_{6,t} + \frac{b_4}{2}\right)^2 + (r_4 - r_{6,m})^2\right]}, \tag{2}$$

with $r_{6,m}$ being the mean radius at the outlet. The axial length of the rotor l_r is:

$$l_r = b_4 + r_4 - r_{6t}, \tag{3}$$

and the radius of curvature of the blade r_c in the tangential plane is:

$$r_c = \frac{l_r}{2\sin\left(\frac{1}{2}(90° - \beta_{6,m})\right)}, \tag{4}$$

whereby the last equation assumes a rotor inlet blade angle equal to 90° valid for all turbines investigated in this paper. $\beta_{6,m}$ is the arithmetic mean value of the relative flow angle at the outlet with the definition of outlet mean values for a variable ϕ given by:

$$\phi_{6,m} = \frac{1}{2}\left(\phi_{6,h} + \phi_{6,t}\right), \tag{5}$$

and the rotor mean values given by:

$$\phi_{R,m} = \frac{1}{2}\left[\phi_4 + \frac{1}{2}\left(\phi_{6,h} + \phi_{6,t}\right)\right]. \tag{6}$$

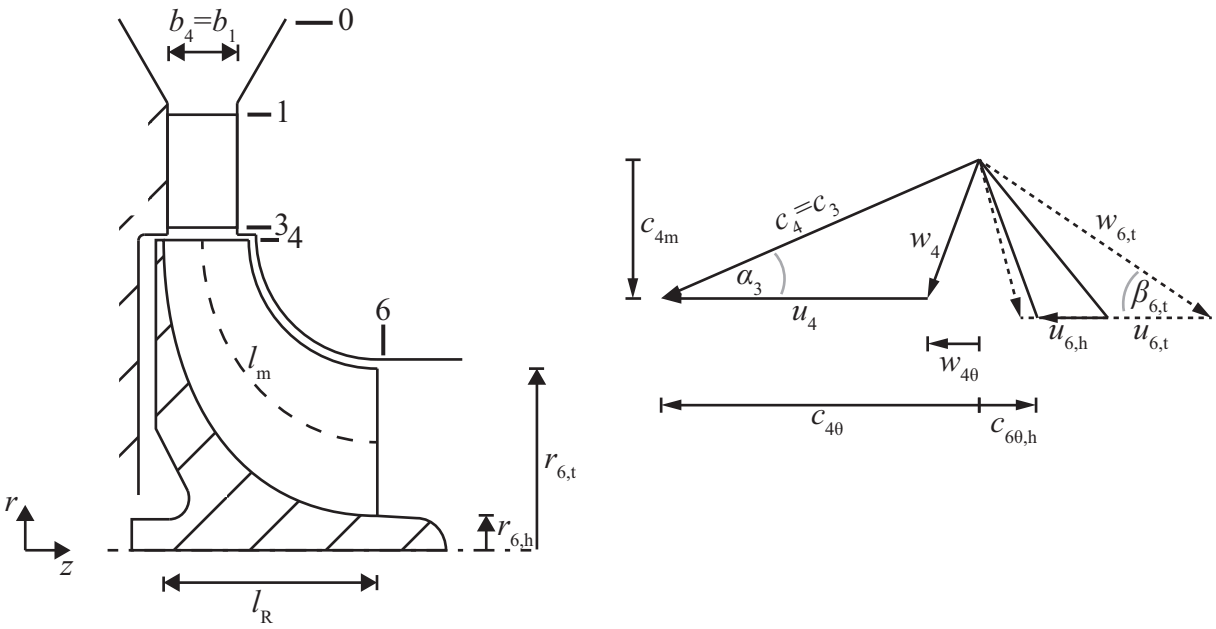


Figure 10: Sketch of a radial turbine with the numbering of the calculation stations and the definition of the velocity triangles together with the absolute flow angle α and the relative flow angle β.

Fluid property routines

The static conditions at the nozzle inlet are deduced from the total inlet conditions and the velocity at State 1 that will later be calculated iteratively (note: all conditions are static if not indicated as total by subscript '0') by:

$$T_1, p_1, \rho_1 = f(p_0, T_0, \Delta h_{0,1s} = -\frac{1}{2}c_1^2). \tag{7}$$

The enthalpy drop from the inlet to the nozzle exit is then related to the isentropic enthalpy change $\Delta h_{1,3s}$ and the nozzle losses $\Delta h_{l,N}$ by:

$$\Delta h_{1,3} = \Delta h_{1,3s} + \Delta h_{l,N}, \tag{8}$$

and the enthalpy drop from the inlet to the outlet is related to the isentropic enthalpy change $\Delta h_{1,6s}$ and the nozzle losses plus the rotor losses $\Delta h_{l,N} + \Delta h_{l,R}$ by:

$$\Delta h_{1,6} = \Delta h_{1,6s} + \Delta h_{l,N} + \Delta h_{l,R}. \tag{9}$$

Note that the sign convention is negative for a drop in enthalpy and losses generally have a positive sign. Then, the pressure at a State j is obtained from the isentropic enthalpy change with:

$$p_j = f(p_1, T_1, \Delta h_{1,js}), \tag{10}$$

and all other fluid values (temperature T, density ρ and speed of sound a) are computed from this pressure and the actual enthalpy change with:

$$T_j, \rho_j, a_j = f(p_1, T_1, p_j, \Delta h_{1,j}). \tag{11}$$

Any equation of state can be used for this purpose. Finally, together with the through-flow area A_j, the meridional velocity is given by:

$$c_{jm} = \frac{\dot{m}}{A_j \rho_j}. \tag{12}$$

Nozzle calculation

For unchoked flow conditions the nozzle inlet velocity c_1 is iteratively calculated from Eq. 12. Thereafter, the nozzle outlet is calculated with an initial guess for c_3 and $\Delta h_{l,N}$ giving the actual enthalpy drop by:

$$\Delta h_{1,3} = -\frac{1}{2}(c_3^2 - c_1^2), \tag{13}$$

and the isentropic enthalpy drop by:

$$\Delta h_{1,3s} = \Delta h_{1,3} - \Delta h_{l,N}. \tag{14}$$

From that the nozzle meridional outlet velocity c_{3m} can be calculated from eqs. 10 - 12. Leading to the absolute outlet velocity:

$$c_3 = \frac{c_{3m}}{\sin(\alpha_3)}. \tag{15}$$

Thereafter, choking conditions must be checked and for unchoked flow conditions the calculation is repeated from Eq. 13 until a converged solution is obtained. However, for choked flow conditions the calculation is repeated right from the beginning with the corrected mass flow:

$$\text{if } c_3 > a \text{ then } c_3 = a, c_{3,m} = c_3 \sin(\alpha_3), \text{ and } \dot{m} = c_{3m}\rho_3 A_3. \tag{16}$$

Finally, the tangential velocity component at the nozzle exit is calculated as:

$$c_{4\theta} = c_{3\theta} = \sqrt{c_3^2 - c_{3m}^2} \tag{17}$$

Rotor outlet calculation

With initial values for $c_{6\theta}$, c_6, $\Delta h_{l,N}$ and $\Delta h_{l,R}$ the specific work w_x is calculate from the Euler work equation as:

$$w_x = u_6 c_{6\theta} - u_4 c_{4\theta}. \tag{18}$$

From that, the actual enthalpy change follows as:

$$\Delta h_{1,6} = w_x - \frac{1}{2}(c_6^2 - c_1^2), \tag{19}$$

and the isentropic enthalpy change as:

$$\Delta h_{1,6s} = \Delta h_{1,6} - \Delta h_{l,N} - \sum \Delta h_{l,R,i}. \tag{20}$$

All information is now available to obtain the density at State 6 from the enthalpy changes in conjunction with Eq. 10 and Eq. 11. This then gives c_{6m} from Eq. 12 which is used to calculate the relative tangential velocity component at the rotor outlet by:

$$w_{6\theta,t/h} = -\frac{c_{6m}}{\tan(\beta_{6,t/h})}. \tag{21}$$

Thereafter, the tangential absolute velocity component at hub and tip is derived from:

$$c_{6\theta,t/h} = w_{6\theta,t/h} + u_{6,t/h}, \tag{22}$$

and the absolute velocity at hub and tip is:

$$c_{6,t/h} = \sqrt{c_{6m}^2 + c_{6\theta,t/h}^2}. \tag{23}$$

The mean values are computed from Eq. 5 to be used in the next iteration step. Since for the investigated operation range the nozzle is choked before the rotor, no examination on rotor choking is conducted. All information is now available to calculate the losses and then repeat the procedure from Eq. 13.

Losses and efficiency calculation

The losses expressed as enthalpy losses can be divided into nozzle losses, leading edge losses, passage losses, tip losses, trailing edge losses, and exit energy losses. Where the last takes into account that the kinetic energy at the exit can not be used to recover static pressure. To calculate the shaft work, also the windage losses in the back chamber and mechanical losses must be taken into account. Since these losses do not change the nozzle or rotor outlet conditions they must not be applied to the flow path analysis. Furthermore, if not otherwise stated these losses are not incorporated in the experimental obtained efficiencies and can not be calculated since information on the geometry of the back chamber is missing.

Nozzle losses

Nozzle vanes can be designed in a way to allow for large incidence angles with minimal incidence losses that are negligible. This is intensified by the low flow velocities at the nozzle inlet. Only passage losses and trailing edge losses have to be considered which are normally combined into one loss model and are calculated according to Baines (2005) by:

$$\Delta h_{l,N} = \zeta \frac{1}{2} c_3^2, \tag{24}$$

where the loss coefficient ζ is defined as:

$$\zeta = \frac{1}{Re^{0.2}} (\tan^2 (90° - \alpha_3) \cdot \frac{l_s}{s} + \frac{o}{b_3}) \tag{25}$$

with l_s being the nozzle vane chord length, s the distance between two adjacently trailing edges. Hence, l_s/s is the solidity given by:

$$\frac{l_s}{s} = \frac{l_s}{2\pi r_3 / N_N} \tag{26}$$

with N_N being the number of nozzle vanes. The Reynolds-number Re is calculated with the fluid properties at the outlet, the absolute velocity at the outlet c_3, and the chord length l_s. o is the throat diameter and is approximated with the sinus rule:

$$o = \sin (\alpha_3)\, s = \sin (\alpha_3)\, \frac{2\pi r_3}{N_N}. \tag{27}$$

Note throughout the paper the properties at State 3 are taken to be equal to State 4.

Rotor incidence losses

Consideration of rotor inlet incidence losses is important since the leading edge is thin and thus the kinetic energy stored in the relative velocity component in tangential direction $w_{4\theta}$ can not be recovered. Therefore, the incidence loss is calculated (see for instance Ventura et al. (2012)) as:

$$\Delta h_{l,R,Inc} = \frac{w_{4\theta}^2}{2}. \tag{28}$$

Rotor tip losses

Radial turbine impellers are most often un-shrouded sometimes called semi-open impellers. Thus, a gap between the blade tip and the casing exists introducing tip losses but no shroud disk friction losses occur. Therefore, the tip losses are calculated with the correlation provided

by Moustapha et al. (2003, pp. 229-230, Eq. 8.40):

$$\Delta h_{l,R,Tip} = \frac{u_4^3 N_R}{8\pi}(K_a \epsilon_a C_a + K_r \epsilon_r C_r + K_{ar}\sqrt{\epsilon_a \epsilon_r C_a C_r})$$

$$\text{with the coefficients beeing}$$

$$K_a = 0.4, K_r = 0.75, K_{ar} = -0.3,$$

$$C_a = \frac{1 - \frac{r_{6,t}}{r_4}}{c_{4m} b_4}, \text{ and}$$

$$C_r = \frac{r_{6,t}}{r_4} \frac{l_r - b_4}{c_{6m} \frac{1}{2}(r_{6,t}^2 - r_{6,h}^2)} \tag{29}$$

with ϵ_a being the axial clearance, ϵ_r being being the radial clearance and l_r being the rotor length defined by Eq. 3. For sake of simplicity some geometric definitions have already been inserted making the equation look slightly different from the original publication.

Passage losses

Calculation of passage losses can be considered as the least intuitive part in the overall loss prediction. This stems mainly from the complexity of defining appropriate geometric parameters which are an equivalent hydraulic diameter, passage length, and curvature radius as well as selecting the important fluid dynamic effects. These are mainly skin friction losses, pressure gradient losses, and trailing edge losses. Since the losses are often directly proportional to the geometry parameters or its inverse values different definitions will have a direct impact on the calculated losses and may require a slight modification to the loss calculation.

In conjunction with the rotor mean values for the relative velocity and the absolute velocity defined by Eq. 6, the passage losses are calculated as:

$$\Delta h_{l,R,Pass} = \frac{1}{2} f \frac{l_m}{D_h} w_{R,m}^2 + 0.7 \frac{2 r_4}{N_R r_c} c_{R,m}^2, \tag{30}$$

with f being the pipe friction factor according to McKoen et al. (1999) defined by:

$$\frac{1}{\sqrt{f}} = 1.930 log_{10}(Re\sqrt{f}) - 0.537, \tag{31}$$

and where:

$$Re = f(p_{R,m}, T_{R,m}, D_h, w_{R,m}). \tag{32}$$

In passing by it is worth noting that the pipe friction factor can also be calculated with a similar equation but with different coefficients given by (Schlichting & Gersten 2003) (p. 551, Eq. 17.130) or the so-called Colebrook-White (Colebrook 1939) equation without having a noticeable impact on the results. However, the extended Colebrook-White equation might be used if surface roughness should be included.

The first term of Eq. 30 takes the skin friction into account and is used similarly by Suhrmann et al. (2010) and Ventura et al. (2012). This is directly deduced from the definition of the pipe friction factor. The second term takes the blade loading into account and a very similar form of this term appeared in a lecture given by Rodgers (1987). But instead of using the blade curvature Rodgers used the rotor passage length but specific information on how to calculate this is not given. Suhrmann et al. (2010) instead applied the curvature and Ventura et al. (2012) followed this approach. Unfortunately, no detailed information on the curvature definition is given. Therefore, in this paper a relatively simple definition of the curvature radius (Eq. 4) is applied and the factor 0.7 in the second term of Eq. 30 is a pure empirical value that was found by comparing calculated efficiencies to measured efficiencies. This factor might change with different definitions of the curvature.

Note trailing edge losses are not separately accounted for and their effect is hidden in one of the other loss models.

Exit losses

Exit diffusers are seldom considered although they can improve the static efficiency by 3 percentage points (Futral & Holeski 1968). Therefore, exit loss are calculated with the assumption that the complete exit kinetic energy is dissipated. This loss is only considered for total-static efficiency calculations by:

$$\Delta h_{l,Exit} = \frac{c_6^2}{2}. \tag{33}$$

Efficiency

The total-inlet to static-outlet efficiency is finally calculate as:

$$\eta_s = \eta_{0,6s} = \frac{\Delta h_{0,6s} + \Delta h_l}{\Delta h_{0,6s}}, \tag{34}$$

with:

$$\Delta h_l = \Delta h_N + \Delta h_{R,Inc} + \Delta h_{R,Tip} + \Delta h_{R,Pass} + \Delta h_{Exit}. \tag{35}$$

Calculation of air equivalent values

Particularly the NASA experimental results are presented as U.S. standard air equivalent values. Calculating these values correctly is crucial for code validation and thus merits a detailed description. The NASA reports give the U.S. standard air temperature as $T_{us} = 518.67$ R $= 288.15$ K and the U.S. standard air pressure as $p_{us} = 14.69$ lb.in^{-2} $= 1.0128 \cdot 10^5$ Pa. Values of the gas const. R and isentropic index γ are not given in the reports, so it is assumed these take the standard values of 0.287 kJ.kg^{-1}.K^{-1} and 1.4 respectively giving an isobaric heat capacity of 1.005 kJ.kg^{-1}.K^{-1}. These are common values and slight changes in air composition have negligible effect. The equivalent values for enthalpy change Δh_{eq}, mass flow rate $\dot{m}_{eq}$, and pressure ratio Π_{eq} can then be calculated from:

$$\Delta h_{eq} = \Delta h / \Theta_{cr} \tag{36}$$

$$\dot{m}_{eq} = \dot{m}\sqrt{\Theta_{cr}} \cdot \epsilon / \delta \tag{37}$$

$$\Pi_{eq} = (\Delta h_{is} \frac{\gamma_{us}}{\gamma_{us} - 1} \frac{1}{R_{us} T_{us}} + 1)^{\frac{\gamma_{us}}{\gamma_{us}-1}} \tag{38}$$

with Δh being the enthalpy change , $\dot{m}$ being the mass flow rate, and Δh_{is} being the isentropic enthalpy change all calculated for instance with a mean-line program. The normalisation factors follow as:

$$\Theta_{cr} = \left(\frac{V_{cr}}{V_{cr,us}}\right)^2 = \left(\frac{\sqrt{\gamma R T_{t,0}}}{\sqrt{\gamma_{us} R_{us} T_{us}}}\right)^2 \tag{39}$$

$$\delta = \frac{p_{t,0}}{p_{us}} \tag{40}$$

$$\epsilon = \frac{\gamma_{us}}{\gamma} \frac{\left(\frac{\gamma+1}{2}\right)^{\frac{\gamma}{\gamma-1}}}{\left(\frac{\gamma_{us}+1}{2}\right)^{\frac{\gamma_{us}}{\gamma_{us}-1}}} \tag{41}$$

Often the total-to-static efficiency and the total-total efficiency are plotted as functions of the tip-to-jet velocity ratio:

$$\nu = u_4 / v_0, \tag{42}$$

with u_4 being the (leading edge) tip blade velocity and v_0 being the spouting velocity calculated with the isentropic enthalpy change between inlet and outlet given by:

$$v_0 = \sqrt{2 \Delta h_{0t,6s}}. \tag{43}$$

These are not converted into equivalent values. Effectively for a fixed turbine geometry the tip-to-jet velocity ratio incorporates changes of rotational speed divided by changes in inlet temperature and pressure ratio. This value has been proven worthy since the static-to-total isentropic efficiency can be approximated with one closed curve that roughly follows a quadratic function.

Appendix B Input values for the mean-line calculations

Table 4 lists all geometry and thermodynamic input values for the mean-line calculations. Most of them have been taken from the original publications and converted into SI units. However, some like the fluid properties have been derived from, e.g., information given on the fluid.

Table 4: Input parameters for mean-line calculations taken from the original publications and converted into SI units if necessary

Turbine:	Kofskey	Wasserbauer	Ricardo B	NASA 1980	Real gases
Figure:	4	4	3	2	5
T_{t0} / K	300.0	338.9	400.0	322.2	varied
p_{t0} / Pa	0.6481E+05	0.3861E+05	varied	1.379E+05	varied
p_6 / Pa	varied	varied	1.0E+05	varied	varied
$n_{100\%}$ / $\frac{1}{\mathrm{s}}$	383.09	496.60	250.0 - 716.7	554.38	varied
r_1 / m	0.0962	0.0734	0.0883	0.0972	0.0972
r_4 / m	0.0765	0.583	0.0635	0.0752	0.0752
r_{6t} / m	0.0545	0.0415	0.0392	0.0472	0.0472
r_{6h} / m	0.0190	0.0145	0.0114	0.0229	0.0229
b_1 / m	0.0196	0.0147	0.0079	0.0081	0.0081
Z_N	14	14	17	29	29
Z_R	11	11	12	12	12
l_s / m	0.0460	0.0351	0.0337	0.0275	0.0275
ϵ_a / m	4.826E-04	2.794E-04	2.540E-04	3.0E-04	3.0E-04
ϵ_r / m	2.540E-04	3.810E-04	2.540E-04	3.0E-04	3.0E-04
α_3 / deg.	18.0	18.0	22.3	15.59	15.59
β_{6t} / deg.	33.3	33.3	32.0	33.77	33.77
β_{6h} / deg.	57.5	57.5	46.0	41.56	41.56
Fluid	Air	Argon	Air	Air	varied
EOS	Perfect gas	Perfect gas	Perfect gas	Perfect gas	REFPROP
R / $\frac{\mathrm{J}}{\mathrm{kg\ K}}$	287.0	208.0	287.0	287.0	-
γ	1.4	1.67	1.4	1.4	-
c_p / $\frac{\mathrm{J}}{\mathrm{kg\ K}}$	1005.0	520.0	1005.0	1005. 0	-
$\mu/10^{-6}$ / $\frac{\mathrm{kg}}{\mathrm{m\ s}}$	18.25	2.2559	18.25	18.25	REFPROP

Appendix C CFD calculations

The CFD calculations are performed in ANSYS CFX and based on the following set-up:

1. Second-order spatial discretisation
2. Steady state assumption
3. One nozzle passage and one rotor passage with periodic boundary conditions
4. Mixing interfaces

5. Mesh refinement in four steps according to Table 5

Table 5: Results from a mesh independence study

Level	Total number of nodes	$\dot{m}$	η_{ts}
Coarse	0.5 Mio.	0.2954	82.37
Medium	1.0 Mio.	0.2950	82.62
Fine	2.4 Mio.	0.2917	82.98
Extra Fine	4.5 Mio.	0.2909	82.95